



Cite this: RSC Adv., 2025, 15, 47161

Catalytic performance of α -MnO₂ nanorods on the degradation of rhodamine B using chlorine dioxide as an oxidant

 Myong-Song Ri, Hyon-Ju Kim, Kyong-Il Kim, Won-Il Song, Yon-Suk Jo and Kyong-Sik Ju *

Manganese dioxide (MnO₂) nanorods were synthesized by a hydrothermal method using manganese sulfate and sodium hypochlorite as raw materials. Manganese dioxide nanorods were characterized by scanning electron microscopy (SEM), X-ray diffraction (XRD), and X-ray photoelectron spectroscopy (XPS). The as-synthesized MnO₂ nanorods were applied to degrade rhodamine B dyes with high concentration in the presence of chlorine dioxide. The catalytic activity was the highest for manganese dioxide nanorods with rod-shaped morphology, a diameter of 80–100 nm, a length of 1.0–1.5 μ m, and a crystal phase of tetragonal α -MnO₂, prepared at 150 °C for a reaction time of 10 h. Under the reaction conditions of a chlorine dioxide concentration of 7.5 mg L⁻¹, a rhodamine B concentration of 50 mg L⁻¹, a reaction time of 30 min, catalyst amounts of 0.60 g L⁻¹ and a pH range of 4–8, the degradation efficiency of rhodamine B approached 99.2%.

Received 18th September 2025

Accepted 11th November 2025

DOI: 10.1039/d5ra07092a

rsc.li/rsc-advances

1 Introduction

Recently, the wastewater of organic compounds such as dyes, pigments, and phenolic compounds has become a major source of environmental pollution. These wastewater sources cause adverse effects to aquatic lives, human health and the environment.^{1–4} Various treatment techniques have been applied to remove organic compounds from wastewater, including automatic variable filtration technology (AVF), chemical oxidation, solvent extraction, membrane techniques, adsorption, advanced photo-oxidation process, coagulation, and biological treatment.^{5–8}

The wet catalytic oxidation process is a mature technology used to remove toxic or non-biodegradable organic pollutants in water and is able to oxidize organic pollutants into carbon dioxide or into products that can be removed by biological treatment.^{9–11} Hydrogen peroxide,^{12,34} ozone,^{13–15} chlorine dioxide^{16–18} and peroxymonosulfate^{19,20,41} are typical oxidants that are widely used in wet catalytic oxidation processes. Here, hydrogen peroxide has the disadvantage of being an expensive and time-consuming oxidant. However, chlorine dioxide is one of the most widely used oxidants because it has strong oxidative ability, does not generate carcinogens such as trichloromethane after oxidation, and is inexpensive.^{21–24}

Recently, with the rapid development of nanotechnology, the catalytic oxidation technology using nanocatalysts has been widely applied toward the treatment of organic pollutants.^{25–27}

High-Tech Research and Development Center, Kim Il Sung University, Pyongyang, Democratic People's Republic of Korea

In particular, MnO₂ nanomaterials have attracted much attention due to their low cost and high catalytic activity.^{28,29} There have been extensive reports on the removal of organic pollutants such as rhodamine B, methylene blue, sulfamethoxazole, and phenol in the presence of manganese dioxide nanomaterials as catalysts.^{28–40}

MnO₂ exists in various forms, such as α -, β -, γ -, δ - and λ -MnO₂, according to the arrangement of octahedral units [MnO₆] at the faces and edges of MnO₂.^{39–41} Among them, α -MnO₂ presented higher oxidation activity than β -MnO₂ and γ -MnO₂ due to its higher surface area, small pore size and strongest oxygen adsorption ability with more exposure of [MnO₆] edges.^{34–39} In particular, it has been reported that α -MnO₂ nanorods exhibit higher oxidative degradation properties of sulfamethoxazole than β -MnO₂ nanorods.⁴⁰

In the literature,⁴¹ it has been reported that the catalytic activity of α -MnO₂ mainly relies on the specific surface area and crystallinity and follows the order of α -MnO₂ nanoflowers > α -MnO₂ nanorods > α -MnO₂ nanoparticles > MnO₂ microparticles. Saputra *et al.* also tested the catalytic activities of different crystallographic MnO₂ (α , β , γ) in peroxymonosulfate solution and found that α -MnO₂ nanowires presented the highest activity, which was attributed to the high surface area and preferable crystalline structure.³⁶

Studies have been reported on the degradation of phenolic derivatives, dyes, *etc.* by ClO₂ in the presence of catalysts, such as CuO_x/Al₂O₃,⁴² CuO_x-La₂O₃/Al₂O₃,^{43,44} NiO-CuO_x-La₂O₃/Al₂O₃,⁴⁵ Al₂O₃ (ref. 46) and MnO₂-carrier.⁴⁷ However, there have been no reports on the removal of organic pollutants by ClO₂ in the presence of MnO₂ nanorod catalysts.

In this paper, we synthesized MnO_2 nanorods using manganese sulphate and sodium hypochlorite as raw materials. In addition, the catalytic performances of MnO_2 nanorods synthesized in different temperatures were investigated in the degradation of rhodamine B by ClO_2 as an oxidant.

2 Experimental

2.1 Catalyst synthesis

Sodium hypochlorite solution (NaClO , Aladdin, 10 wt%), manganese sulphate ($\text{MnSO}_4 \cdot \text{H}_2\text{O}$, Aladdin, 99.5%), sodium hydroxide (NaOH , Aladdin, 99.5%), and sulfuric acid (H_2SO_4 , Aladdin, 99.5%) were used as starting materials. The ClO_2 stock solution was stored under dark conditions at 5 °C and was standardized before using. All reagents are analytical grade and can be used without further purification. Rhodamine B (RhB) was chosen as the organic pollutant. The synthetic equation of the MnO_2 nanorods is as follows.



Initially, 0.02 mol of MnSO_4 was dissolved in a 250 mL glass flask that contained 50 mL of deionized water and then 0.02 mol of NaClO solution was added with stirring. It was transferred to a 100 mL Teflon liner. The Teflon liner was loaded into a stainless steel autoclave and heated in an oven. The autoclave was heated to 150 °C and kept at this temperature for 10 h. Finally, the autoclave was cooled to room temperature naturally. The obtained precipitates were filtered, washed with distilled water and then dried in vacuum at 70 °C for 4 h.

In order to synthesize MnO_2 nanorods with different diameters, the reaction temperature was varied from 110 °C to 190 °C, while the other reaction conditions were kept constant. The obtained catalysts were marked as MnO_2 -110, MnO_2 -130, MnO_2 -150, MnO_2 -170, and MnO_2 -190, corresponding to 110, 130, 150, 170 and 190 °C, respectively.

2.2 Characterization of physical properties

To study the crystallographic properties of the catalysts, XRD analysis was carried out with a D/max-RB X-ray diffractometer with the $\text{Cu K}\alpha$ X-ray source at 40 kV and 100 mA. The morphology and microstructure of the catalysts were further studied by SEM (JSM-6610A, JEOL, JAPAN). The chemical bonding of the catalysts was studied by X-ray photoelectron spectroscopy (ESCALAB-250 carried out with a monochromatic $\text{Al K}\alpha$ (1486.6 eV) radiation source).

2.3 Catalytic characterization

The degradation experiments of RhB using MnO_2 nanorod catalysts were carried out in a 100 mL stoppered Erlenmeyer flask. Firstly, 100 mg of MnO_2 nanorods catalyst and 10 mL of distilled water were placed in a 100 mL stoppered Erlenmeyer flask and dispersed by ultrasonic agitation for 5 min, and then 50 mL of 100 mg L^{-1} RhB solution was added and stirred for 5 min. The pH of the solution was adjusted with sodium hydroxide and sulfuric acid solution. A certain volume of

100 mg L^{-1} chlorine dioxide solution was added to the flask and the volume was calibrated with distilled water. During the reaction, the temperature of the suspension was kept at 20 ± 2 °C. At regular time intervals, 1 mL of the mixed suspension was taken by a syringe and centrifuged to separate the catalyst. At this time, 0.1 mL of 1.0 mol L^{-1} sodium thiosulfate solution was added to the sample to stop the oxidation reaction. The absorbance of the dissolved RhB solution was then measured by UV-Vis spectrophotometer at 552 nm, corresponding to the maximum absorption peak, and the degradation efficiency was calculated.

The degradation efficiency is expressed as follows:

$$\eta = (C_0 - C) \times 100/C_0 \quad (2)$$

where C_0 is the initial concentration and C is the concentration measured at each time interval. In addition, RhB degradation experiments were carried out in the absence and presence of MnO_2 nanorod catalysts.

3 Results and discussion

3.1 Physical characterization

The phase of the as-synthesized MnO_2 nanoparticles was characterized by XRD (Fig. 1).

The sample of manganese dioxide synthesized at 110 °C showed no significant peaks, indicating the presence of amorphous manganese dioxide (Fig. 1a). The diffraction peaks of the MnO_2 nanorods synthesized at 130 and 150 °C appeared at $2\theta = 12.6^\circ, 18.0^\circ, 25.5^\circ, 28.6^\circ, 37.4^\circ, 41.7^\circ, 49.7^\circ, 55.9^\circ, 59.8^\circ, 65.4^\circ$, and 68.8° , which could be indexed as the (110), (200), (220), (310), (211), (301), (411), (600), (521), (002) planes of tetragonal $\alpha\text{-MnO}_2$ (JCPDS no.44-0141), respectively (Fig. 1b and c).

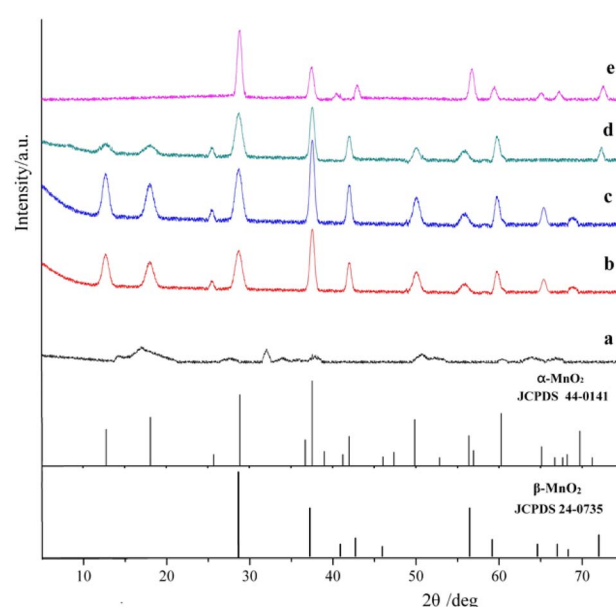


Fig. 1 XRD patterns of the MnO_2 nanoparticles synthesized at different temperatures. (a) 110 °C, (b) 130 °C, (c) 150 °C, (d) 170 °C, (e) 190 °C.

However, the strength increased with increasing temperature, indicating that the crystallinity increased with increasing temperature. At 170 °C, the intensity of α -MnO₂ at 12.6°, 18.0°, 37.4° significantly decreased, indicating that α -MnO₂ starts to transform into β -MnO₂ (Fig. 1d). The diffraction peaks of MnO₂ nanorods synthesized at 190 °C appeared at $2\theta = 28.63^\circ, 37.32^\circ, 42.81^\circ, 56.65^\circ, 59.33^\circ$, and 72.4° , which could be indexed as the (110), (101), (111), (211), (220), (112) planes of tetragonal β -MnO₂ (JCPDS no.24-735), respectively (Fig. 1e). No peaks for any impurities are observed, indicating the high purity of the synthesized product.

In general, the catalytic activity of α -MnO₂ is higher than that of β -MnO₂.³⁴⁻³⁹ Among α -MnO₂ nanomaterials, the catalytic activity follows the order of α -MnO₂ nanoflowers > α -MnO₂ nanorods > α -MnO₂ nanoparticles > MnO₂ microparticles.⁴¹ Thus, the catalytic activity of manganese dioxide synthesized at 150 °C may be the highest.

The morphologies of the as-synthesized MnO₂ were characterized by SEM (Fig. 2).

As can be seen in Fig. 1, when the reaction temperature is lower, the obtained MnO₂ particles are spherical. However, at higher reaction temperatures, the particles become rod-like and both their diameter and length increase. The MnO₂ synthesized at 110 °C consists of MnO₂ nanoparticles with a diameter of 150–200 nm and small amounts of nanorods (Fig. 2a). However, at >130 °C, MnO₂ nanorods were synthesized. The MnO₂ nanorods synthesized at 130–170 °C have a diameter of 70–100 nm and length of 1–1.5 μ m (Fig. 2b–d). In contrast, the MnO₂ nanorods synthesized at 190 °C have a diameter of 150–170 nm and length of 1.5–2 μ m (Fig. 2e). This shows that the reaction temperature is the most important factor in MnO₂ nanorod synthesis.

Among the manganese dioxides synthesized from 130 °C to 170 °C, the manganese dioxide synthesized at 130 °C has the largest specific surface area, while those synthesized at 150 and 170 °C have no significant differences. However, based on XRD and SEM results, it may be concluded that manganese dioxide synthesized at 130 °C has a small particle size but a low

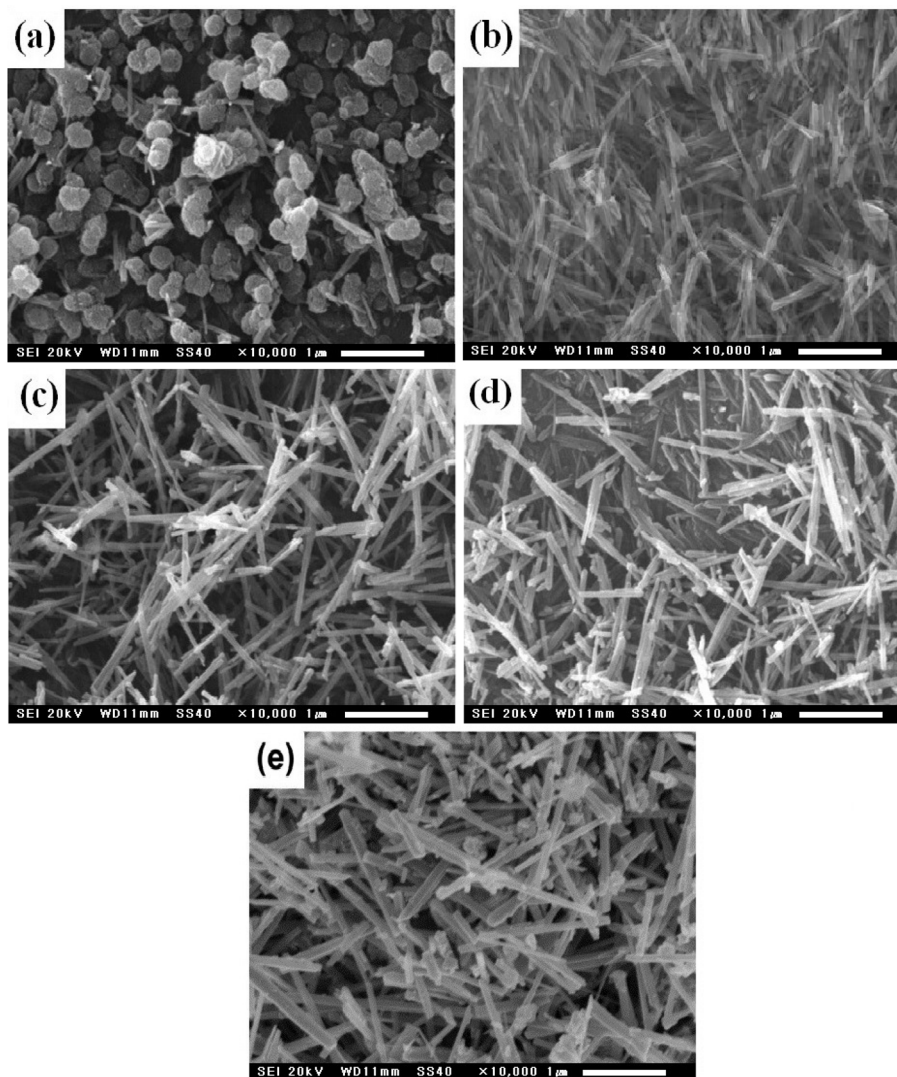


Fig. 2 SEM images of the MnO₂ nanoparticles synthesized at different temperatures. (a) 110 °C, (b) 130 °C, (c) 150 °C, (d) 170 °C, (e) 190 °C.



crystallinity, and the catalytic activity is lower than that of α -MnO₂ synthesized at 150 °C.

The chemical bonding properties of the catalyst were studied by X-ray photoelectron spectroscopy. X-ray photoelectron spectroscopy is a good technology to study the relative composition of the synthesized material and the oxidation state of the manganese ion.

The wide-scan X-ray photoelectron spectra, and the deconvolution of the Mn 2p and O 1s spectra of the as-prepared α -MnO₂ are presented in Fig. 3a-c. The peaks of Mn 2p_{1/2} (654.0 eV) and Mn 2p_{3/2} (641.8 eV) have a spin energy separation of about 12.2 eV, which reveals the presence of Mn⁴⁺ ions in α -MnO₂ (Fig. 3a and b).^{34,49} In the deconvolution of the Mn 2p spectrum (Fig. 3b), the Mn 2p_{3/2} peak is resolved into two components with binding energies centered at 641.8 and 643.6 eV, indicating the presence of the Mn(III) and Mn(IV) oxidation states, respectively. The obtained binding energies match well with previous literature studies.^{49,50} The deconvolution of the O 1s spectrum resulted in two peaks at 529.7 and 531.5 eV for the α -MnO₂ nanorod. As reported in the previous

literature,^{50,51} the peak at the binding energy of 529.4–530.0 eV is assigned to lattice oxygen (in the form of O²⁻), and the peak at 531.3–531.8 eV is assigned to the surface adsorbed oxygen (such as OH). Therefore, in the case of oxygen (Fig. 3c), the two different peaks centered at 529.7 and 531.5 eV correspond to lattice oxygen (in the form of O²⁻) and surface adsorbed oxygen (such as OH), respectively.

3.2 Effect of several factors on the catalytic performance

In order to investigate the catalytic performance of the MnO₂ nanorods synthesized at different temperatures, RhB was selected as the organic pollutant to be degraded in the presence of ClO₂.

3.2.1 Effect of the ClO₂ concentration on the RhB degradation. Using the MnO₂ nanocatalysts synthesized at different temperatures, it is very important to examine the effect on RhB degradation. The effect of the ClO₂ concentration on the RhB degradation process using MnO₂ nanoparticles synthesized at different temperatures was studied using the following experimental conditions: RhB concentration of 50 mg L⁻¹, catalyst

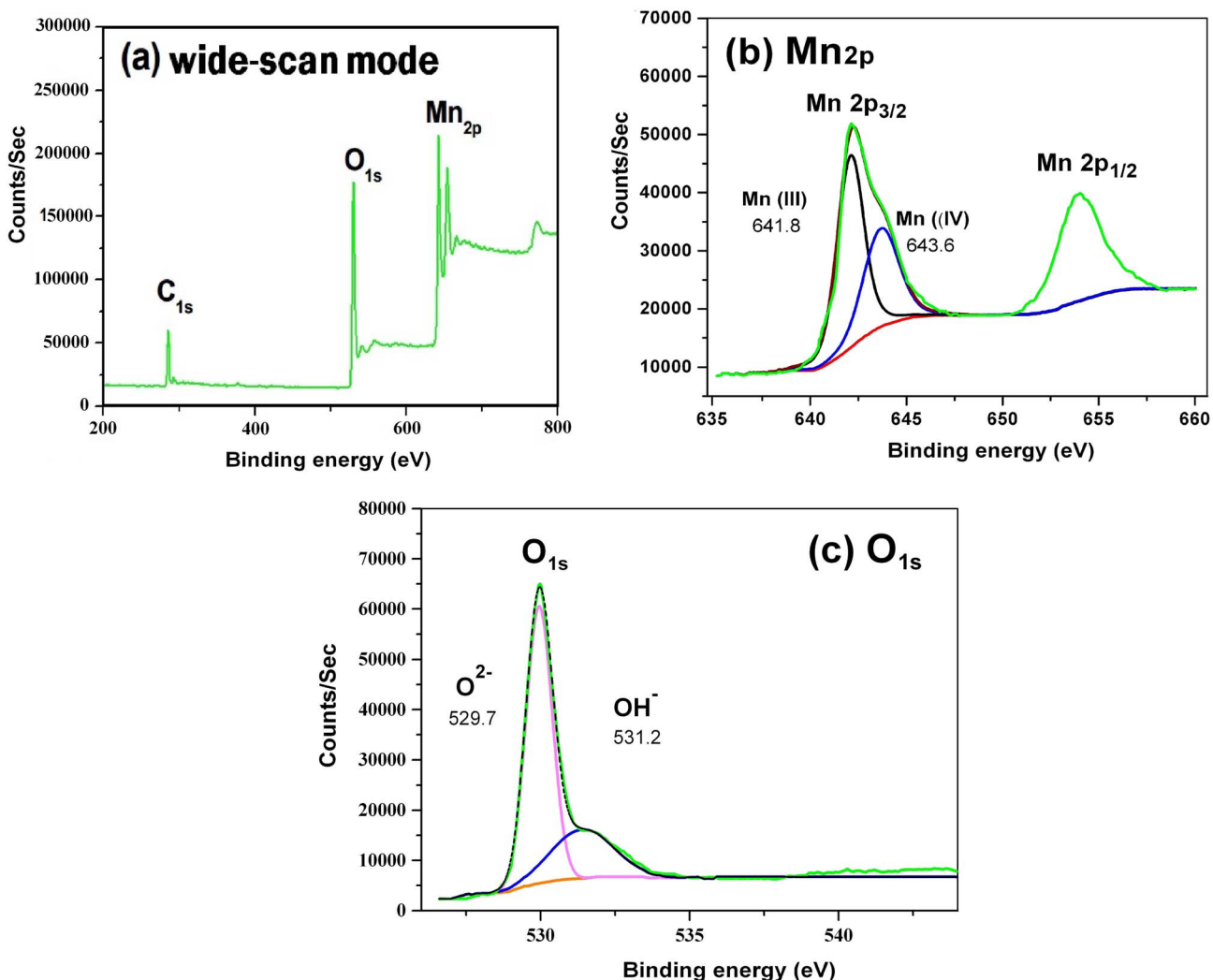


Fig. 3 X-ray photoelectron spectra for the α -MnO₂ nanorods (150 °C and 10 h): (a) wide-scan mode, (b) Mn 2p, and (c) O 1s.

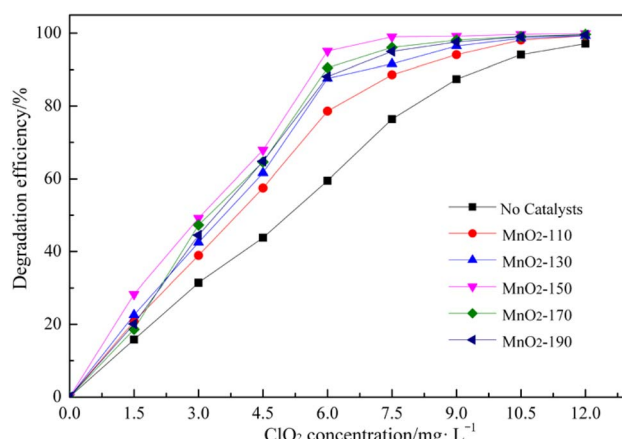


Fig. 4 Effect of the ClO_2 concentration in the RhB degradation process using the MnO_2 nanoparticles synthesized at different temperatures. (reaction conditions: $\text{RhB} = 50 \text{ mg L}^{-1}$, catalysts = 0.8 g L^{-1} , time = 60 min, pH = 6.0, reaction temperature 20°C , MnO_2 -110, MnO_2 -130, MnO_2 -150, MnO_2 -170, MnO_2 -190 catalysts are MnO_2 nanoparticles that were synthesized at 110, 130, 150, 170 and 190 $^\circ\text{C}$, respectively, for 10 h).

amounts of 0.8 g L^{-1} , reaction time of 60 min, reaction temperature of 20°C and pH 6.0.

The results clearly showed that ClO_2 could oxidize RhB (Fig. 4). However, with the MnO_2 nanorod catalysts, the degradation efficiency of RhB was higher than that without catalyst. In particular, in the case of the MnO_2 -150 nanorod, the degradation efficiency of RhB was highest compared to other catalysts. In the absence of the catalyst, the degradation efficiency was the lowest. This is because the MnO_2 nanorods synthesized at 150°C are α - MnO_2 . α - MnO_2 can have oxidation transformation processes of $\text{Mn}^{4+} \rightarrow \text{Mn}^{3+} \rightarrow \text{Mn}^{2+}$, while β - MnO_2 only has one process of $\text{Mn}^{4+} \rightarrow \text{Mn}^{3+}$. Comparing the structures of α - and β - MnO_2 , the two-tunnel structured α - MnO_2 will show higher activity than the single-tunnel structured β - MnO_2 due to the greater exposure of MnO_6 edges. This is consistent with previous literature studies^{19,20} that have reported that α - MnO_2 exhibits higher catalytic oxidation than β - MnO_2 .

When the concentration of chlorine dioxide is 7.5 mg L^{-1} with the addition of the MnO_2 -150 catalyst, 99.0% of RhB is removed for 60 min. This is greater than the degradation efficiency (97.1%) when the chlorine dioxide concentration is 12 mg L^{-1} without the addition of a catalyst.

The effectiveness of a catalyst is that the total cost can be reduced by lowering the oxidant concentration. It also can effectively reduce the environmental pollution by residual chlorine dioxide, which can be caused by the increase of chlorine dioxide dosage. Thus, the chosen catalyst was α - MnO_2 nanorod synthesized at 150°C , and the optimum chlorine dioxide concentration was 7.5 mg L^{-1} with the RhB degradation efficiency above 99%.

3.2.2 Effect of different amounts of catalyst. The effect of the reaction time on the RhB degradation process in the presence of different amounts of MnO_2 nanorods (MnO_2 -150) was performed using the following experimental conditions: RhB

concentration of 50 mg L^{-1} , ClO_2 concentration of 7.5 mg L^{-1} , pH of 6.0, reaction temperature of 20°C .

Fig. 5 shows the degradation efficiency of RhB as a function of the reaction time under different amounts of catalyst conditions, and Fig. 6 shows the UV-Vis absorption spectra of the ($\text{RhB} + \text{ClO}_2 + \text{MnO}_2$ nanorods) solution as a function of time after ClO_2 is added. In the ClO_2 catalytic oxidation process with MnO_2 nanorods, the degradation efficiency of RhB increases rapidly with the reaction time. Also, as the catalyst amounts increased, the degradation efficiency of RhB increases. The degradation efficiency reached more than 70% after 10 min, and reached more than 99% after 30 min. Also, when the catalyst loading was higher than 0.6 g L^{-1} , the degradation efficiency did not significantly increase.

As shown in Fig. 6, the maximum absorption peak of RhB at 552 nm and of ClO_2 at 360 nm were initially observed. Upon increasing the reaction time, the maximum absorption intensity of RhB and ClO_2 decreased. This shows that RhB was effectively removed. Therefore, the catalytic amounts and RhB

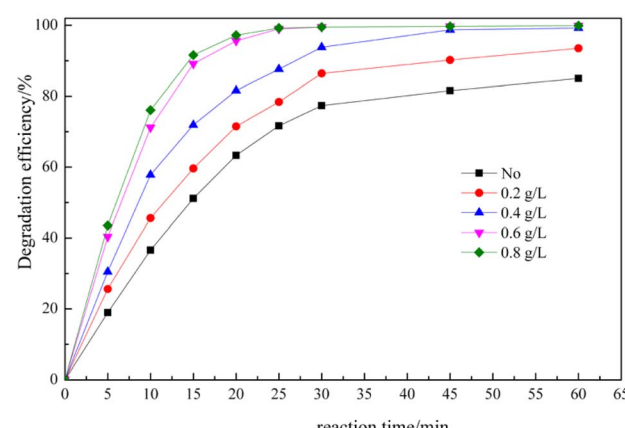


Fig. 5 Effect of the reaction time on the degradation efficiency in the RhB degradation process with different amounts of the MnO_2 nanorod catalyst (MnO_2 -150). (reaction conditions: $\text{RhB} = 50 \text{ mg L}^{-1}$, $\text{ClO}_2 = 7.5 \text{ mg L}^{-1}$, pH = 6.0, and reaction temperature 20°C).

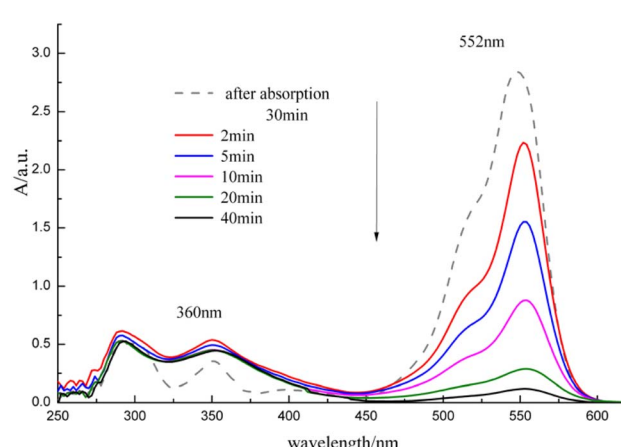


Fig. 6 UV-Vis absorption spectra of the ($\text{RhB} + \text{ClO}_2 + \text{MnO}_2$ nanorods) solution as a function of time after ClO_2 is added.

degradation time were set to 0.6 g L^{-1} and 30 min, respectively. The experimental results show that the MnO_2 nanorod catalyst not only improves the degradation rate of RhB but also shortens the reaction time, which indicates that the ClO_2 catalytic oxidation process has more advantages in engineering applications.

3.2.3 Effect of pH. The pH value is one of the most important factor in the ClO_2 catalytic oxidation because the redox potential of chlorine dioxide and the degradation principle of MB differ with pH. The effect of pH values on the RhB degradation process was studied using the following experimental conditions: RhB concentration of 50 mg L^{-1} , ClO_2 concentration of 7.5 mg L^{-1} , MnO_2 -150 catalyst amounts of 0.6 g L^{-1} , reaction time of 30 min, reaction temperature of 20°C .

Fig. 7 shows that the RhB degradation efficiency by ClO_2 catalytic oxidation strongly depends on pH. When the pH value is 4–8, the degradation efficiency of RhB did not change. However, at pH > 8, the degradation efficiency is small. This is because at pH 4–8, the chemical reaction involves chlorine dioxide reacting with organic pollutants to convert chlorite ions. In contrast, at pH > 9, chlorine dioxide reacts with hydroxyl anions to form chlorite ions and chlorate ions. Chlorite and chlorate ions have a lower oxidation capacity compared to chlorine dioxide.



However, the pH of wastewater is usually 4–9, so it is considered that it does not affect the removal of organic pollutants in real environmental conditions.

3.2.4 Effect of temperature. In general, the effect of temperature on chemical reactions is one of the important factors. As the temperature increases, the rate of chemical

reactions increases, which affects the overall chemical reactions. The dependence of the rate constant (k) on the reaction temperature can be expressed by the Arrhenius equation:

$$\ln(k) = \ln(A) - E_a/RT \quad (5)$$

where A = frequency factor, E_a = activation energy, R = universal gas constant ($8.315 \text{ J K}^{-1} \text{ mol}^{-1}$), and T = absolute temperature (K).

The effect of temperature on the RhB decomposition process was studied by varying the reaction temperature under the following conditions: RhB of 50 mg L^{-1} , chlorine dioxide of 7.5 mg L^{-1} , catalyst amount of 0.60 g L^{-1} , and pH 6.0.

As shown in Fig. 8, the degradation efficiency of RhB increases with increasing temperature. However, the degradation efficiency does not differ significantly within the reaction temperature range of 20 – 30°C . At 20°C , the degradation efficiency of RhB was 99.1% for 30 min. The reaction temperature increases, and the rate of RhB decomposition by chlorine dioxide increases. However, when the temperature is raised above 35°C , the vapor pressure of chlorine dioxide increases, which evaporates rapidly and the decomposition rate increases. In addition, it requires a lot of energy to raise the temperature of wastewater above 30°C . This indicates that the optimum temperature for the degradation reaction of RhB by chlorine dioxide is 20 – 30°C . Therefore, the reaction temperature was chosen to be 20°C .

3.3 Kinetics on the chlorine dioxide catalytic oxidation

3.3.1 Degradation pathways of RhB by chlorine dioxide.

Chlorine dioxide is mainly converted into chlorite anions and chloride anions during redox reactions.^{52–54} The assumed reaction pathways for the degradation of RhB by chlorine dioxide are shown in Fig. 9.

Chlorine dioxide is highly reactive with amine compounds, especially with tertiary amines with high electron density on nitrogen atoms.⁵³ Therefore, chlorine dioxide may first attack

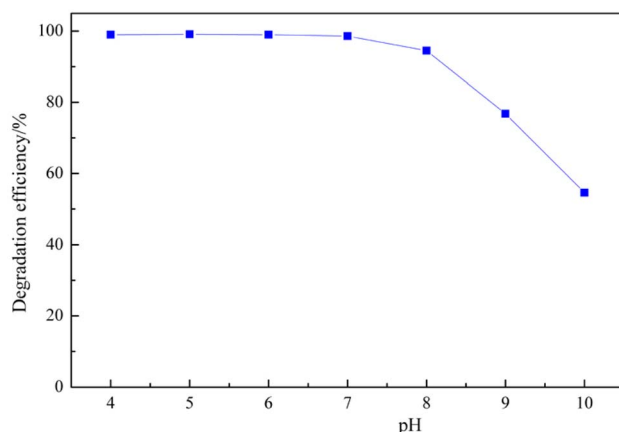


Fig. 7 Degradation efficiency of RhB by chlorine dioxide with different pH values. (reaction conditions: RhB = 50 mg L^{-1} , ClO_2 = 7.5 mg L^{-1} , MnO_2 -150 catalyst = 0.6 g L^{-1} , time = 30 min, reaction temperature 20°C).

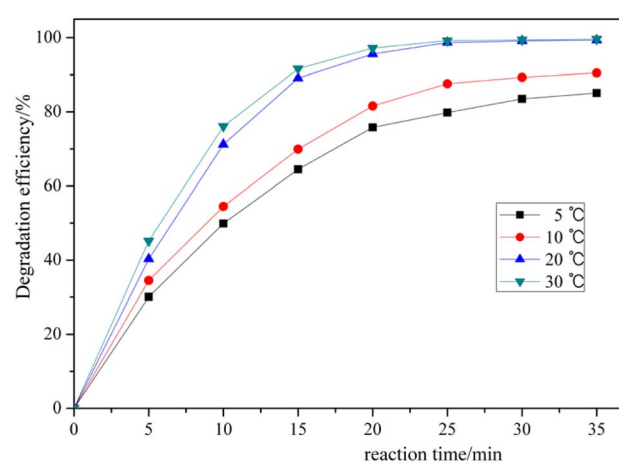


Fig. 8 Degradation efficiency of RhB by chlorine dioxide at different reaction temperatures. (reaction conditions: RhB = 50 mg L^{-1} , ClO_2 = 7.5 mg L^{-1} , MnO_2 -150 catalyst = 0.6 g L^{-1} , and pH = 6.0).

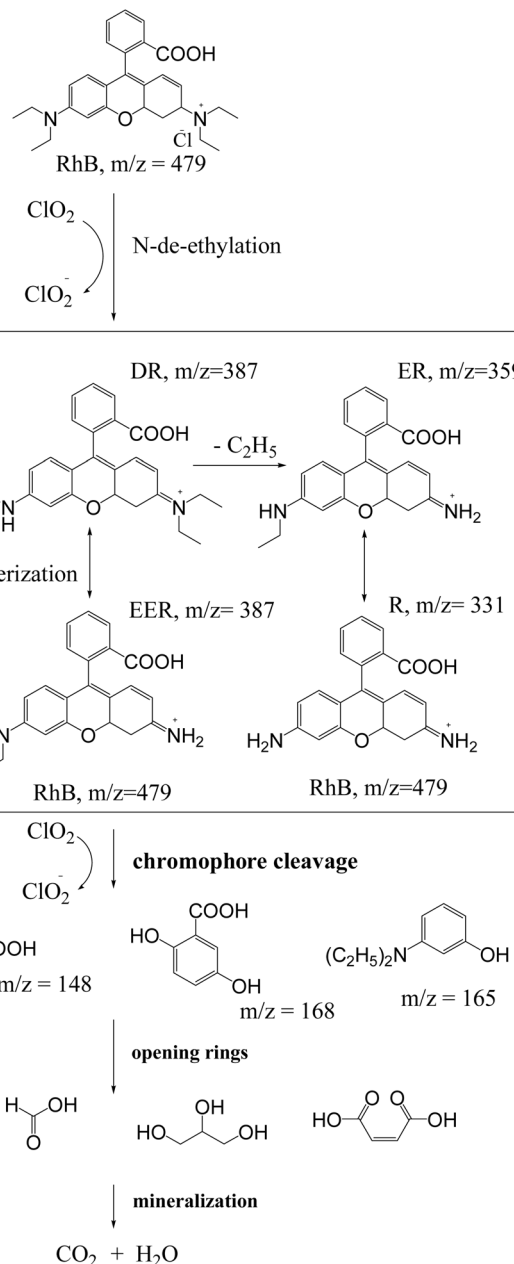


Fig. 9 Assumed degradation pathways of RhB by chlorine dioxide.

the tertiary amine backbone on the side chain of RhB and undergoes the N-de-ethylation reaction. During the reaction, chlorine dioxide is reduced to chlorite anions.^{18,54} Then, the central carbon atom, which forms a conjugated double bond, is attacked to initiate chromophore cleavage reactions, followed by ring opening, and mineralization reactions. The oxidation products formed after the chromophore cleavage reactions may be 3-(diethylamino)phenol, 2-(2,5-dihydroxyphenyl)acetic acid and 2-vinylbenzoic acid. Then these products may be decomposed into small molecular materials such as hydroquinone, malonic acid, oxalic acid, formic acid, and gradually into mineralized products such as CO_2 and H_2O during the ring opening reaction.

3.3.2 Kinetic study of the RhB degradation reaction. The ClO_2 catalytic oxidation of organic compounds generally follows the kinetics of the second-order reaction.⁴⁸ For the kinetic study of the reaction of RhB degradation by chlorine dioxide, the initial concentration of chlorine dioxide was chosen to be more than five times that of RhB. Then, the reaction rate equation is as follows.

$$\frac{d[\text{RhB}]}{dt} = -k_{\text{app}}[\text{ClO}_2]^m[\text{RhB}]^n = -k'[\text{RhB}]^n \quad (6)$$

Here, $[\text{ClO}_2]$ and $[\text{RhB}]$ are the concentrations of chlorine dioxide and RhB, m and n are the orders with respect to the



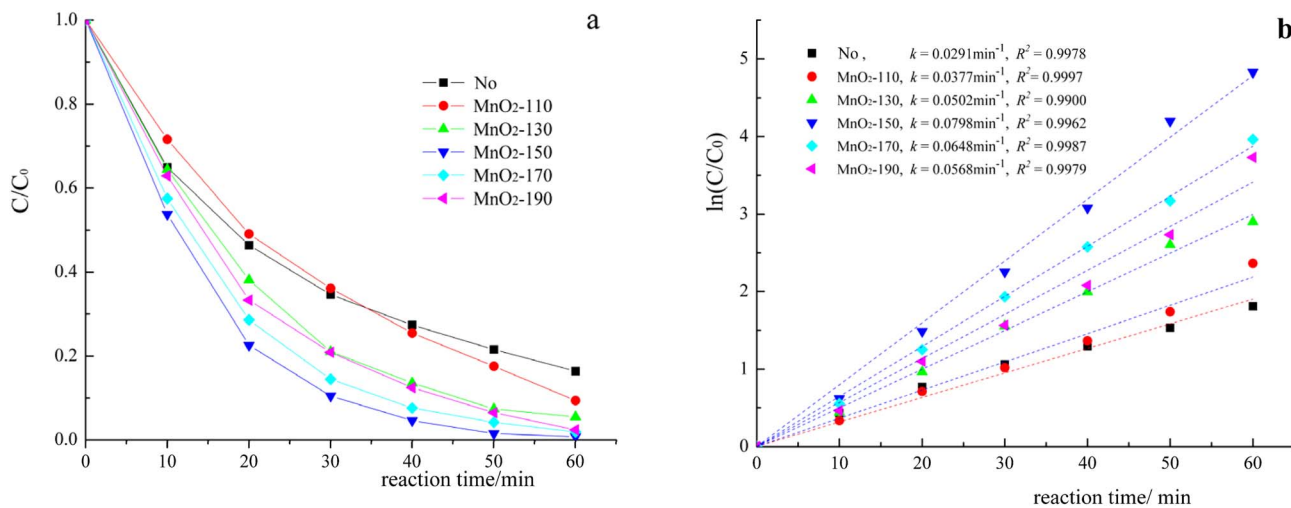


Fig. 10 RhB degradation (a) and kinetic experiments (b) by chlorine dioxide catalytic oxidation using No (without catalyst), MnO₂-110, MnO₂-130, MnO₂-150, MnO₂-170, and MnO₂-190 catalysts. (chlorine dioxide 7.5 mg L⁻¹, RhB 50 mg L⁻¹, catalyst amounts 0.60 g L⁻¹, pH 6.0, and reaction temperature 20 ± 1 °C).

Table 1 Characterization of catalysts for the rhodamine B degradation reaction

Catalyst	Catalyst preparation condition	Degradation condition	Degradation efficiency/%	Ref.
α -MnO ₂ nanorods	180 mg of MnCl ₂ ·4H ₂ O, 127 mM KMnO ₄ 5 mL, 85 °C, 90 min	RhB 20 mg L ⁻¹ = 50 mL, 30% H ₂ O ₂ = 6 mL, α -MnO ₂ = 10 mg, 10 min, pH 4–6	97.5	34
Co Fe ₂ O ₄ /TNTs	3.83 mmol of Co(NO ₃) ₂ ·6H ₂ O, 7.66 mmol of Fe(NO ₃) ₃ ·9H ₂ O, 7.66 mmol of citric acid 150 °C, 16 h	RhB = 100 mg L ⁻¹ , oxone = 4000 mg L ⁻¹ , catalyst = 200 mg L ⁻¹ , pH = 10, time = 20 min	99	55
Co ₃ O ₄ /C	Black Co ₃ O ₄ -based magnetic carbonaceous nanocomposite (MCN)	RhB = 50 mg L ⁻¹ , oxone = 250 mg L ⁻¹ , MCN = 50 mg L ⁻¹ , temperature = 25 °C, time = 1 h	95	56
5GO-FePO ₄ composite	A specific amount of graphite oxide, 2.29 g NH ₄ H ₂ PO ₄ , 5.36 g Fe(NO ₃) ₃ , 800 °C for 4 h	RhB = 10 mg L ⁻¹ , H ₂ O ₂ = 10 mmol L ⁻¹ , catalyst = 1 g L ⁻¹ , time = 120 min, pH = 2.18–10.40	96.99	57
CoFe/SBA-15	10Co9.5Fe/SBA-15-700	RhB = 5.0 mg L ⁻¹ , PMS/RhB molar ratio = 20 : 1, catalyst = 0.10 g L ⁻¹ , temperature = 25 °C, time = 2 h	95	58
Cu/Al ₂ O ₃ /g-C ₃ N ₄ composite	Cu ₁₂ /Al ₂ O ₃ /C ₃ N ₄	RhB = 20 mg L ⁻¹ , H ₂ O ₂ = 10 mmol L ⁻¹ , catalyst = 1.0 g L ⁻¹ , temperature = 25 °C, pH = 4.9, time = 2 h	96.4	59
Fe ₂ O ₃ -Kaolin	Kaolin 2 g, 0.2 mol L ⁻¹ Na ₂ CO ₃ , 0.4 mol L ⁻¹ Fe(NO ₃) ₃ , 400 °C, 3 h	RhB = 15.0 mg L ⁻¹ , H ₂ O ₂ = 0.05 mol L ⁻¹ , catalyst = 1.0 g L ⁻¹ , pH = 2.21, time = 120 min	98	60
Cu-dopedLaTiO ₃ CNTs	LaTi _{0.4} Cu _{0.6} O ₃ Lengths 0.5–2 μ m diameters 30–50 nm	RhB = 8 mg L ⁻¹ , H ₂ O ₂ = 0.02 mol L ⁻¹ , catalyst = 1.4 g L ⁻¹ , time = 120 min RhB = 20 mg L ⁻¹ , PS = 119.0 mg L ⁻¹ , CNT = 0.2 g L ⁻¹ , pH = 3–9 time = 150 min	94	61
Ag@CuO nanocomposite	1.0 g Cu ₂ (OH) ₂ CO ₃ , 0.5 g silver nitrate, 20 mL water, 300 °C for 24 h	RhB = 10 mg L ⁻¹ , PS = 200 mg L ⁻¹ , Ag@CuO = 0.5 g L ⁻¹ , DMPO = 100 mmol L ⁻¹ , time = 30 min	100	62
SDS@Fe ₃ O ₄	FeCl ₃ ·6H ₂ O (0.40 M), FeCl ₂ ·4H ₂ O (0.20 M), SDS (0.10 M), 300 mL of DI water, 200 mL of 25% NH ₄ OH	RhB = 10 mg L ⁻¹ , H ₂ O ₂ = 2.0 \times 10 ⁻¹ mol L ⁻¹ , SDS@Fe ₃ O ₄ = 0.1% w/v, pH = 3, temperature = 25 ± 2 °C	98	63
α -MnO ₂ nanorods	Diameter of nanorods: 80–100 nm, length of nanorods: 1.0 to 1.5 μ m	RhB = 50 mg L ⁻¹ , ClO ₂ = 7.5 mg L ⁻¹ , α -MnO ₂ = 0.6 g L ⁻¹ , time = 40 min, pH = 4–9	99.7	This study



concentrations of ClO_2 and RhB, respectively, and k_{app} is the apparent rate constant.

Kinetic studies of the RhB degradation reactions with different catalysts were carried out and the results are shown in Fig. 10.

Fig. 10a and b show the oxidative degradation of RhB using No catalyst, MnO_2 -110, MnO_2 -130, MnO_2 -150, MnO_2 -170, MnO_2 -190 catalysts in the presence of chlorine dioxide (7.5 mg L^{-1} of ClO_2 , 50 mg L^{-1} of RhB, 0.60 g L^{-1} of catalyst addition, pH 6.50). The degradation efficiency of RhB during 30 min varies according to the different catalysts: MnO_2 -150 (99.2%) > MnO_2 -170 (97.5%) > MnO_2 -190 (91.7%) > MnO_2 -130 (82.5%) > MnO_2 -110 (74.5%) (Fig. 10a). In addition, the rate constants were estimated to be 0.0291, 0.0377, 0.0502, 0.0798, 0.0648, and 0.0568 min^{-1} for the M-0(No catalyst), MnO_2 -110, MnO_2 -130, MnO_2 -150, MnO_2 -170 and MnO_2 -190 (Fig. 10b). The results indicate that the rate constants of ClO_2 oxidation process on RhB are found to be significantly different with the catalyst, indicating that the MnO_2 nanorods synthesized 150 °C are very effective oxidation catalysts (Table 1).

4 Conclusions

In this paper, the effect of MnO_2 nanorods synthesized with manganese sulfate and sodium hypochlorite as precursors on the degradation of RhB by chlorine dioxide was studied. The characterization results showed that the morphology of MnO_2 synthesized at 150 °C is rod shape, the diameter of MnO_2 nanorods ranged from 80 to 100 nm and the length ranged from 1.0 to 1.5 μm , and crystal phase of tetragonal α - MnO_2 . The catalytic activity of MnO_2 nanorods was investigated in terms of the degradation of RhB by ClO_2 catalytic oxidation. In the degradation condition of ClO_2 concentration 7.5 mg L^{-1} , RhB concentration 50 mg L^{-1} , reaction time 30 min, catalyst amounts 0.60 g L^{-1} and pH 6 ± 2 , RhB degradation efficiency was up to 99.2% by the catalytic effect of the MnO_2 nanorod. It shows that MnO_2 nanorod is very reasonable to remove RhB in wastewater.

Author contributions

Myong-Song Ri: investigation, writing, experiment. Hyon-Ju Kim: experiment. Kyong-Il Kim: writing – review & editing. Won-Il Song: writing – original draft. Yon-Suk Jo: formal analysis. Kyong-Sik Ju: conceptualization, methodology, investigation.

Conflicts of interest

There are no conflicts to declare.

Data availability

The data that support the findings of this study are available from the corresponding authors upon reasonable request. The results presented in the study have been obtained by using the chlorine dioxide catalytic oxidation experiments.

Acknowledgements

This work was supported by the State Commission of Science and Technology in DPR Korea.

References

- H. S. Naik, P. M. Sah, S. B. Dhage, S. G. Gite, R. W. Raut, *Modern Approaches in Waste Bioremediation Environmental Microbiology*, 2023, 265–298.
- L. Handojo, D. Pramudita, D. Mangindaan and A. Indarto, *Microorganisms for Sustainability*, 2020, **18**, 45–76.
- J. Huang, Z. Huang, T. Liu, Y. Wen, J. Yuan, S. Yang and H. Li, *Chinese Chem. Lett.*, 2025, **36**, 110179.
- K. Sharma, S. Kalita, N. S. Sarma and A. Devi, *RSC Adv.*, 2020, **10**, 1925–1936.
- S. Maity, D. Sinha, A. Sarkar, *Nanotechnology in the Life Sciences*, 2020, 299–313.
- T. Liu, J. Huang, Z. Huang, Q. Luo, H. Wu, Y. Meng, C. He and H. Li, *Chem. Eng. J.*, 2024, **486**, 150209.
- S. Anandan, V. K. Ponnusamy and M. Ashokkumar, *Ultrason. Sonochem.*, 2020, **67**, 105130.
- S. A. Bhat, F. Sher, M. Hameed, O. Bashir, R. Kumar, D. V. N. Vo, P. Ahmad and E. C. Lima, *Chemosphere*, 2022, **288**, 132606.
- F. E. Titchou, H. Zazou, H. Afanga, J. E. Gaayda, R. A. Akbour, P. V. Nidheesh and M. Hamdani, *Chem. Eng. Process.- Process Intensification*, 2021, **169**, 108631.
- I. Fatimah, G. Fadillah, I. Yanti and R. Doong, *Nanomaterials*, 2022, **825**(12), 1–34.
- W. J. Sun, H. X. Lu, L. Ma, X. D. Tan, C. Y. Jin, H. L. Wu, L. L. Chen, M. Y. Liu, H. Z. Wei and C. L. Sun, *J. Environ. Sci.*, 2022, **120**, 105–114.
- M. Ashrafivala, S. B. Mousavi, S. Z. Heris, M. Heidari, M. Mohammadpourfard and H. Aslani, *Int. J. Hydrogen Energ.*, 2022, **47**, 33530–33540.
- P. Li, S. J. Zhan, L. Yao, Y. Xiong and S. H. Tian, *J. Hazard. Mater.*, 2022, **437**, 129235.
- H. J. Wang, J. H. Zhan, L. W. Gao, G. Yu, S. Komarneni and Y. J. Wang, *J. Hazard. Mater.*, 2020, **390**, 122180.
- K. Okamoto, R. Urushidate, S. Shimoda, K. Suzuki, A. Fukuoka and T. Takada, *Carbon Reports*, 2024, **3**, 142–148.
- M. Y. Xu, Y. L. Lin, T. Y. Zhang, C. Y. Hu, Y. L. Tang, J. Deng and B. Xu, *J. Hazard. Mater.*, 2022, **436**, 129195.
- K. Hupperich, X. A. M. Mutke, M. S. Abdighahroudi, M. Jütte, T. C. Schmidt and H. V. Lutze, *Environ. Sci.-Water Res. Technol.*, 2020, **6**(9), 2597–2606.
- B. J. Liu, C. R. Qin, F. Q. Zhang, S. Wang, C. Liang, S. X. Nie, S. F. Wang and S. Q. Yao, *ACS Omega*, 2020, **5**, 22475–22481.
- S. O. Ganiyu, S. Sable and M. G. El-Din, *Chem. Eng. J.*, 2022, **429**, 132492.
- H. X. Wei, J. J. Zhao, B. Shang and J. Zhai, *J. Environ. Chem. Eng.*, 2022, **10**, 108532.
- C. T. Wang, Q. Wang, Q. H. He and Z. F. Zhou, *Dyestuffs Coloration*, 2006, **43**, 49–55.
- L. S. Shi, H. M. Zhu, Y. Y. Dong and Y. Y. Li, *J. Shandong Univ. (Eng. Sci.)*, 2006, **36**, 91–95.

23 C. T. Wang, Q. H. He and P. He, *Environ. Sci. Technol.*, 2006, **29**, 65–67.

24 W. Gan, Y. Ge, Y. Zhong and X. Yang, *Environ. Sci.: Water Res. Technol.*, 2020, **6**(9), 2287–2312.

25 S. L. Chiam, S. Y. Pung and F. Y. Yeoh, *Environ. Sci. Pollut. Res.*, 2020, **27**(6), 5759–5778.

26 Z. Q. Cai, Y. M. Sun, W. Liu, F. Pan, P. Z. Sun and J. Fu, *Environ. Sci. Pollut. Res.*, 2017, **24**, 15882–15904.

27 A. Kusior, K. Michalec, P. Jelen and M. Radecka, *Appl. Surf. Sci.*, 2019, **476**, 342–352.

28 C. L. Yu, G. Li, L. F. Wei, Q. Z. Fan, Q. Shu and J. C. Yu, *Catal. Today*, 2014, **224**, 154–162.

29 W. X. Zhang, Z. H. Yang, X. Wang, Y. C. Zhang, X. G. Wen and S. H. Yang, *Catal. Commun.*, 2006, **7**, 408–412.

30 H. J. Cui, H. Z. Huang, M. L. Fu, B. L. Yuan and W. Pearl, *Catal. Commun.*, 2011, **12**, 1339–1343.

31 S. Sandip and P. Anjali, *Sep. Purif. Technol.*, 2014, **134**, 26–36.

32 K. D. Lin, W. P. Liu and J. Gan, *Environ. Sci. Technol.*, 2009, **43**, 3860–3864.

33 G. Chen, L. Zhao and Y. H. Dong, *J. Hazard. Mater.*, 2011, **193**, 128–138.

34 S. M. Wang, A. O. Guan, J. H. Wang, X. F. Fu, X. Guo, Y. Tian, K. X. Wang, W. P. Cao and C. M. Zhao, *Bull. Mater. Sci.*, 2022, **45**, 35–42.

35 H. Salari, M. Erami, M. H. Dokooohaki and A. R. Zolghadr, *J. Mol. Liq.*, 2022, **345**, 117016–117027.

36 E. Saputra, S. Muhammad, H. Q. Sun, H. M. Ang, M. O. Tade and S. B. Wang, *Environ. Sci. Technol.*, 2013, **47**, 5882–5887.

37 Y. T. Meng, W. Q. Song, H. Huang, Z. Ren, S. Y. Chen and S. L. Suib, *J. Am. Chem. Soc.*, 2014, **136**, 11452–11464.

38 H. Yuan, L. J. Wang, Z. Chen, B. Shen, J. S. Wei, P. Zeng and X. H. Wen, *Sci. Total Environ.*, 2021, **785**, 147328–147336.

39 Y. M. Dong, K. Li, P. P. Jiang, G. L. Wang, H. Y. Miao, J. J. Zhang and C. Zhang, *RSC Adv.*, 2014, **4**, 39167–39173.

40 J. L. Wan, L. Zhou, H. P. Deng, F. L. Zhan and R. J. Zhang, *J. Mol. Catal. A: Chem.*, 2015, **407**, 67–74.

41 J. Deng, Y. J. Ge, C. Q. Tan, H. Y. Wang, Q. S. Li, S. Q. Zhou and K. J. Zhang, *Chem. Eng. J.*, 2017, **330**, 1385–1419.

42 X. Y. Bi, P. Wang, H. Jiang, H. Y. Xu, S. J. Shi and J. L. Huang, *J. Environ. Sci.*, 2007, **19**, 1510–1515.

43 X. Y. Bi, P. Wang, C. Y. Jiao and H. L. Cao, *J. Hazard. Mater.*, 2009, **168**, 895–900.

44 X. Y. Bi, P. Wang, H. Jiang, H. Y. Xu, S. J. Shi and J. L. Huang, *J. Hazard. Mater.*, 2008, **154**, 543–549.

45 L. J. Huang, T. Xu and S. F. Wang, *Asian J. Chem.*, 2012, **24**(4), 1727–1730.

46 H. L. Wang, J. Dong and W. F. Jiang, *J. Hazard. Mater.*, 2010, **183**, 347–352.

47 F. J. Yu and L. S. Shi, *J. Shandong Univ. (Eng. Sci.)*, 2010, **40**(2), 88–94.

48 F. Tian, Z. M. Qiang, C. Liu, T. Zhang and B. Z. Dong, *Chemosphere*, 2010, **79**, 646–651.

49 F. W. Boyom-Tatchemo, F. Devred, G. Ndiffo-Yemeli, S. Laminsi and E. M. Gaigneaux, *Appl. Catal. B: Environ.*, 2020, **260**, 118159.

50 R. E. John, A. Chandran, M. Thomas, J. Jose and K. C. George, *Appl. Surf. Sci.*, 2016, **367**, 1–21.

51 P. Mahamallik, S. Saha and A. Pal, *Chem.-Eng. J.*, 2015, **276**, 155.

52 W. H. Gan, S. R. Huang, Y. X. Ge, T. Bond, P. Westerhoff, J. X. Zhai and X. Yang, *Water Res.*, 2019, **159**, 348–357.

53 D. H. Rosenblatt, L. A. Hull, D. C. De Luca, G. T. Davis, R. C. Weglein and H. K. R. Williams, *J. Am. Chem. Soc.*, 1967, **89**(5), 1158–1163.

54 J. Wen, M. Aeschbacher, E. Salhi, S. Canonica, U. V. Gunten and M. Sander, *Environ. Sci. Technol.*, 2013, **47**, 11147–11156.

55 Y. Du, W. Ma, P. Liu, B. Zou and J. Ma, *J. Hazard. Mater.*, 2016, **308**, 58–66.

56 K. Y. Lin, H. A. Chang and R. C. Chen, *Chemosphere*, 2015, **130**, 66–72.

57 G. Sheng, Z. Gaoke and C. Y. Jimmy, *J. Colloid Interf. Sci.*, 2015, **448**, 460–466.

58 L. X. Hu, F. Yang, L. P. Zou, H. Yuan and X. Hu, *Chinese J. Catal.*, 2015, **36**, 1785–1797.

59 C. S. Zhou, Z. D. Liu, L. J. Fang, Y. L. Guo, Y. P. Feng and M. Yang, *Catalysts*, 2020, **10**, 317.

60 S. Guo, G. Zhang and J. Wang, *J. Colloid Interf. Sci.*, 2014, **433**, 1–8.

61 L. Zhang, Y. Nie, C. Hu and J. Qu, *Appl. Catal. B: Environ.*, 2012, **125**, 418–424.

62 S. H. Chen, L. Y. Ma, Y. G. Du, W. Zhan, T. C. Zhang and D. Y. Du, *Sep. Purif. Technol.*, 2021, **256**, 117788.

63 T. Zhang, T. T. Zhou, L. He, D. Q. Xu and L. Bai, *Synthetic Met.*, 2020, **267**, 116479.

64 M. S. Ansari, K. Raees, M. A. Khan, M. Z. A. Rafiquee and M. Otero, *Polymers*, 2020, **12**, 2246.